DOI 10.24425/aee.2023.145421

Research on the influence of power frequency electric field of pantograph on passengers' health in high-speed EMU

RUI TIAN✉, **JIA-QI ZHANG**, **MAI LU**

Key Laboratory of Opto-Electronic Technology and Intelligent Control of Ministry of Education
Lanzhou Jiaotong University
Gansu Province, China
e-mail: {✉*tianrui_2014/zhangjiaqi_529}@126.com, mai.lu@hotmail.com*

(Received: 01.11.2022, revised: 08.02.2023)

Abstract: In this work we discussed the safety of the electric field environment in the No.3 carriage where the pantograph is located. DSA380 pantograph, CRH5 EMU carriage and passengers' models were established to study the electric field exposure of passengers at different positions. The results showed that $\boldsymbol{E}_{\max}$ in the carriage without passengers is 1.173×10^6 mV/m. Then we set the passengers' positions according to the electric field distribution in the carriage without passengers and obtained that $\boldsymbol{E}_{\max}$ in the carriage with passengers is 3.195×10^6 mV/m. It can be seen that the maximum induced electric field intensity of passengers at different positions appears on the soles of shoes, the maximum value is 3.028×10^5 mV/m, the maximum induced current density occurs at the ankle, its maximum value is 3.476×10^{-5} A/m^2. It can be concluded that the maximum induced electric field intensity of passenger's head appears in the cerebrospinal fluid area, with a maximum value of 202.817 mV/m, and the maximum induced electric field intensity of passenger's head at the door is larger than that in the middle of the carriage. The maximum values of the induced electric field intensity in all tissues of passengers are much smaller than the basic limits of electromagnetic exposure to the public set by the International Commission on Non-Ionizing Radiation Protection (ICNIRP). This study indicated that the pantograph has little influence on the electric field environment in the carriage under working state, and will not cause any health hazard to the passengers in this working frequency electric field environment.

Key words: induced current density, induced electric field intensity, high-speed EMU, pantograph, power frequency electric field

1. Introduction

In order to further promote social and economic development, build a more efficient and modern integrated railroad transportation system, the Medium and Long-Term Railway Network Plan (2016) was released by China National Railway Group Co. The document points out that the road network structure will be further optimized, the scale of railroad coverage will be expanded, and the scale of the railroad will reach 175 000 km by 2025, including 38 000 km of high-speed railroads [1]. A high-speed electric multiple unit (EMU) has increasingly become the main force of China's transportation. At present, the traction system of a high-speed EMU generally adopts the AC drive mode, which is mainly composed of a pantograph, main circuit breaker, traction transformer, traction converter, traction motor and so on. The power configuration is the distributed power type of five motors and three trailers [2]. Pantographs are installed on the top of No. 3 and No. 6 carriages of the EMU. Generally, only one pantograph is in a working state when the whole EMU is running, and the other one is reserved for standby. As an important part of the traction system of a high-speed EMU, a pantograph is used to contact with the traction catenary for current collection. After current collection, 25 kV high-voltage AC is transmitted to the traction transformer through high-voltage cables, main circuit breakers, grounding switches, current sensors and other traction system equipment, so as to change the voltage to 1770 V AC to supply power to the traction/auxiliary circuits [2], making the train operate stably. A pantograph plays a vital role in a high-speed EMU.

However, in the current collection process of a high-speed EMU traction system, except that the high-voltage cable directly connected to the pantograph and the insulator under the pantograph base have shielding and high-voltage insulation functions, the pantograph itself is directly exposed in the air without any shielding measures. A pantograph, as the equipotential device of the catenary, also has 25 kV high voltage, which will generate a strong electric field in the surrounding space, and these electric fields in the EMU carriage may cause potential harm to the health of passengers and train staff.

In view of the influence of electromagnetic fields on human beings and animals, how to make rational use of electromagnetic fields to benefit mankind have been the subject of continuous attention and research by scholars in recent years. Mai Lu *et al*. designed a multi-channel transcranial magnetic stimulation system (mTMS) in 2009, and obtained the induced current density and electric field distribution in the real human head model based on anatomy for the first time through the mTMS method, providing a promising focused deep brain stimulation method [3]. Jiang Xing *et al*. detected the location of hemorrhagic stroke hemorrhage by the microwave forward scattering method, using the change in the gain S_{21} and phase $\varphi_{s_{21}}$ difference value of a transceiver antenna and the change in the electric field distribution value of the brain in a cerebral hemorrhage state and normal brain state [4]. Xiaolin Huo *et al*. studied the acute beneficial effect of electric field stimulation on secondary inflammatory response in rats with spinal cord injury, the results showed that the electric field through the spinal cord was approximately 270 mV/mm, and this large applied electric field helped to counteract the Ca^{2+} flux at the injury site, confirming the acute beneficial effect of electric field stimulation on the secondary inflammatory response [5]. Takashi Ohtsuki *et al*. found that the electric field exposure therapy of 30 minutes a day for 5 consecutive days has a therapeutic effect on young people's sleep disorders through a control experiment [6].

While actively exploring the positive effects of electromagnetic fields on organisms, researchers have also drawn some neutral conclusions. For example, Grzegorz Cieslar *et al*. exposed rats to electrostatic fields with intensities of 16 kV/m and 25 kV/m for 56 consecutive days (8 hours per day) to study the effects of electrostatic fields generated near high-voltage DC transmission lines on four behaviors, including locomotor activity, exploratory activity, space learning and irritability, and showed that a transient and significant decrease in locomotor activity occurs at the beginning of exposure, while other behaviors do not show any effect, and the changes in behavioral characteristics are more pronounced in rats exposed to 25 kV/m electrostatic fields [7]. Wang Songcen *et al*. established an equivalent circuit model of the electric vehicle wireless charging system, and set up a control group to detect the number and concentration of white blood cells in each group of mice, the results showed that under the experimental conditions of 50 kHz working frequency and 100 W input power, the electromagnetic field would not affect the immune system of mice [8].

But at the same time, electromagnetic fields may also bring certain risks and hazards to human health. For example, reference [9] found that by investigating the impact of mobile phone microwave radiation on postpartum newborns, the average fetal platelet volume of pregnant women who use mobile phones more than 60 minutes a day during pregnancy is lower than normal, and the levels of C-reactive protein, calcitonin, troponin and lactic acid are higher than normal. In reference [10], researchers carried out epidemiological investigation on 263 soldiers working in a high-frequency radar station of a base, and the results showed that high-frequency electromagnetic radiation had a negative impact on the reproductive health of soldiers. Regrettably, the research on the electric field environment of a high-speed EMU pantograph is currently focused on the electromagnetic radiation characteristics of pantograph catenary arc discharge [11,12] by domestic and foreign scholars, without considering that the pantograph itself is a charged body and no electromagnetic shielding measures have been taken by the pantograph itself, therefore, the environmental analysis of the induced electric field generated by the high-speed EMU pantograph under working state and the evaluation of the electric field exposure of passengers in the carriage are still lacking.

In this work, a full-scale model of the DSA380 pantograph was built on the top of a high-speed EMU by using SolidWorks, 3D modeling software, and an EMU carriage model as well as a five-layer head ball body model were built by using COMSOL Multiphysics, simulation analysis software [13], all geometric models were integrated into COMSOL Multiphysics. The induced electric field intensity and induced current density in different body tissues of passengers at different positions in the carriage were calculated and analyzed, and finally compared the simulation results with the standards related to public exposure in the ICNIRP (International Commission on Non-Ionizing Radiation Protection) [14], studied and evaluated the influence of power frequency electric field distribution generated by pantographs after the current collection of a 25 kV high-voltage catenary on the electric field environment in the carriage and the safety of human health.

2. Principle of electric field

With the development of high-speed EMU technology, the electrical and electronic equipment with high power, high sensitivity and a high transmission rate used by the EMU is becoming increasingly intelligent. There is a lot of electrically charged work equipment in the EMU, so

the electromagnetic components generated in the carriage are more and more complex [15]. It is difficult to directly measure the electric field inside the human body in real time [16]. The epidemiological survey, which is one of the traditional methods for electric field exposure safety assessment, takes a long time, and creates a large database [17], which makes it difficult to provide data support for high speed EMU electric field exposure safety assessment in a short period. Therefore, an effective method is to use numerical simulation to study the influence of a low-frequency electric field on different tissues of passengers' bodies.

In the process of contact and current collection between a pantograph and a 25 kV high-voltage catenary, the pantograph itself will generate a power-frequency electric field. The frequency of high-voltage alternating current received by the pantograph is 50 Hz, and its wavelength size (6 000 km) is much larger than the size of the EMU body, so the power frequency electric field generated around the pantograph can be regarded as a quasi-static electric field.

In this work, the following formulas, (1)–(2), can be used to calculate the distribution of space electric fields, and thus the value of the induced electric field and induced current in human tissues can be obtained. In addition, taking into account the presence of various media, one more constitutive equation is required, as shown in (3):

$$\boldsymbol{E} = -\nabla\varphi, \tag{1}$$

$$\nabla \cdot \boldsymbol{E} = \frac{\rho}{\varepsilon}, \tag{2}$$

$$\boldsymbol{J} = \sigma\boldsymbol{E}, \tag{3}$$

where: $\boldsymbol{E}$ is the electric field intensity (V/m), φ is the electric potential (V), ∇ is the Hamiltonian operator, ρ is the charge body density (C/m^3), ε is the dielectric constant (F/m), $\boldsymbol{J}$ is the current density (A/m^2), σ is conductivity (S/m).

The required boundary condition is shown in Formula (4):

$$\nabla \times \boldsymbol{E} = 0. \tag{4}$$

3. Simulation model establishment

3.1. Human model

In order to truly and effectively calculate the relevant values in different tissues of passenger bodies in a high-speed EMU, the authors constructed a 1 755 mm standing human body model using COMSOL Multiphysics, according to the relevant indexes in GB/T 10000-88 [18]. To make the results more accurate, the three-layer cerebral model [19, 20], which was used in previous common electromagnetic exposure studies, was further optimized. In this work, a five-layer ellipsoidal model of the human head was used, including five structures: scalp, skull, cerebrospinal fluid, gray matter and white matter. The thickness of each tissue layer is the difference of the corresponding ellipsoidal radius, Fig. 1, and their specific dimensional parameters are shown in Table 1 [13, 21, 22].

The upper part of the torso is made of a spliced structure with a rectangular body, three cylinders and two spheres, the height and width of the main part of the rectangular body are 598 mm and 445 mm, respectively. The length of the conical arms is 526 mm.

Table 1. Related size parameters of five-layer ellipsoidal model of human head

Tissue name	radius/mm		
	a	b	c
Scalp	118	96	81
Skull	111	89	74
Cerebrospinal fluid	106	84	69
Gray matter	104.8	82.8	67.8
White matter	101.8	79.8	64.8

The lower part of the torso also adopts the splicing structure, and the leg is a cone with a length of 848 mm. The human foot is formed by the equivalent combination of two half-cylinders and a rectangular body. The geometric model of the human body in the standing position is shown in Fig. 1.

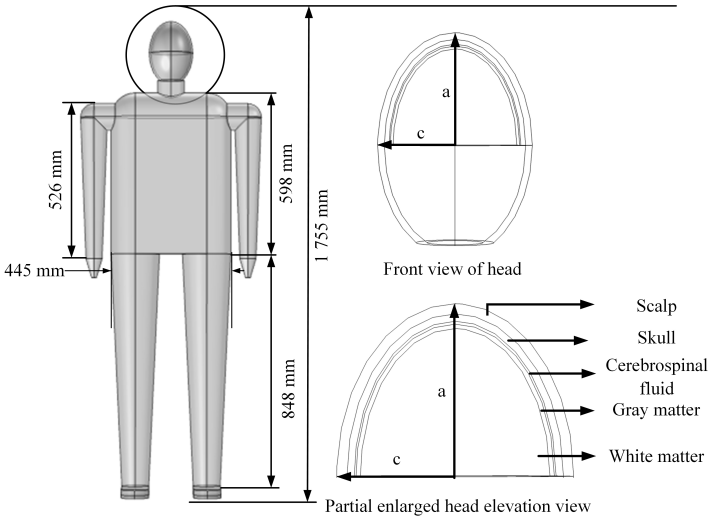

Fig. 1. Standing human body model

The calculation cannot be performed by constructing the geometric model alone, but it also requires setting up the relative permittivity and conductivity of different tissues of the human body. To extract and calculate the dielectric parameters of human tissues, the 4th-order Cole-Cole model [23] is generally used internationally. Assuming that the human tissue is homogeneous and isotropic [24], the frequency of the electric field generated by the pantograph after receiving the current is 50 Hz, and the relative permittivity and conductivity of different human tissues at this frequency are shown in Table 2 [13]. The data related to the human torso were taken as the arithmetic mean of bones, fat and muscle [19].

Table 2. Dielectric parameters and electrical conductivity of different human tissues

Tissue name	Relative dielectric constant	Conductivity (S/m)
Scalp	5.127×10^4	4.272×10^{-4}
Skull	8.868×10^3	2.006×10^{-2}
Cerebrospinal fluid	1.09×10^2	2
Gray matter	1.211×10^7	7.526×10^{-2}
White matter	5.290×10^6	5.327×10^{-2}
Bones	8.868×10^3	2.006×10^{-1}
Fat	1.473×10^6	1.956×10^{-2}
Muscle	1.772×10^7	2.333×10^{-1}

3.2. Modeling of pantograph and EMU carriage

3.2.1. Pantograph modeling

In this work, according to the basic parameters and design requirements of the DSA 380 pantograph [25], 3D modeling software, SolidWorks, was used to construct the model of the DSA 380 pantograph.

There are small parts on the pantograph that affect the number of grid units, such as orifices and chamfers. Because these small parts are far away from a wavelength of 50 Hz AC and will not affect the distribution of the power frequency electric field around the pantograph, some parts of the pantograph are simplified after considering the calculation accuracy and scale of the model comprehensively. The overall assembly diagram of the pantograph after simplification is shown in Fig. 2.

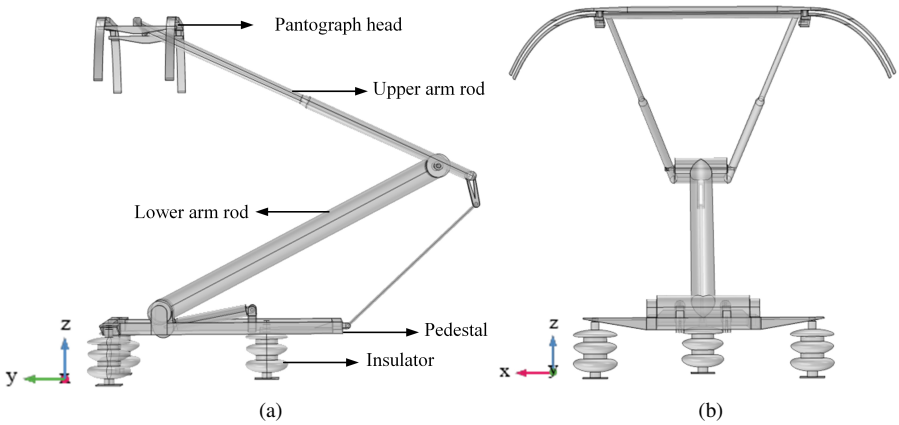

Fig. 2. Assembly drawing of pantograph: side view of pantograph (a); front view of pantograph (b)

3.2.2. Modeling of EMU carriage

Without affecting the realism and validity of the simulation, a carriage model with a length of 7 760 mm, a width of 3 200 mm and a height of 2 730 mm was constructed and discussed in this paper, taking carriage No. 3 with a pantograph as an example. The main body of the carriage is made of aluminum alloy with a wall thickness of 50 mm. At the same time, the roof deflector of CRH5 was simulated on the top of the carriage body. The thickness of the roof deflector is 50 mm, and the material is the same as the main body of the carriage, which is aluminum alloy. All the parameters of the carriage, windows and the roof deflector are from CRH5 EMU [2].

3.3. Human body, carriage and air domain models

In this paper, the pantograph model, human body model and EMU carriage model were integrated in COMSOL. This work studied the electromagnetic environment inside the carriage, while the radiation source pantograph is outside the carriage, so an air domain is used to wrap the models. A hemispherical air domain with a radius of 7 500 mm was set up. The coordinates of the four passengers' positions in the carriage are shown in Table 3.

Table 3. Position coordinates of passengers in carriage

Passenger	Passenger overhead coordinates	Passenger	Passenger overhead coordinates
Passenger A	(1 600, 1 920, 1 805)	Passenger C	(300, 7 182, 1 805)
Passenger B	(1 600, 5 583.5, 1 805)	Passenger D	(2 900, 7 182, 1 805)

The pantograph receives current through contact with the contact network, and its voltage is set to 25 kV. At the same time, the bottom of the insulator and the surface of the carriage are set as grounding conditions. Combining the initial conditions and boundary conditions, the overall model is finely meshed for dissection. Finally, the degree of freedom of solution of this model is 853 482, and the calculation is carried out with a 32 G memory computer. Figure 3 shows

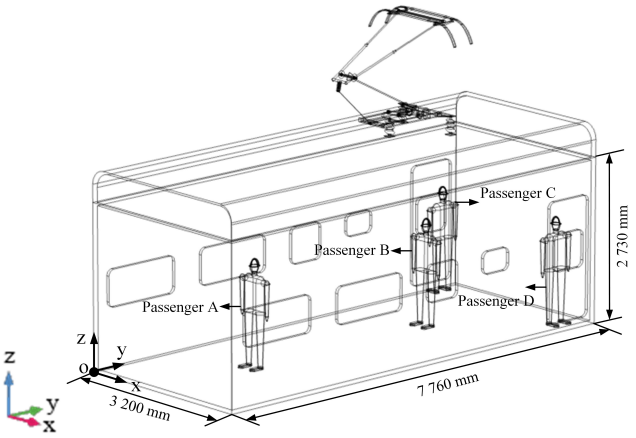

Fig. 3(a)

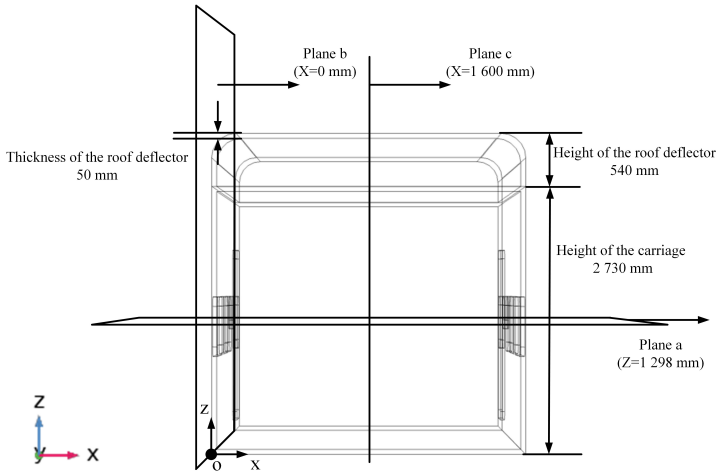

(b)

Fig. 3. Overall model diagram of EMU (a); front view of carriage (b)

the overall model of the EMU carriage. Figure 4 shows the grid partition of the EMU and the pantograph model.

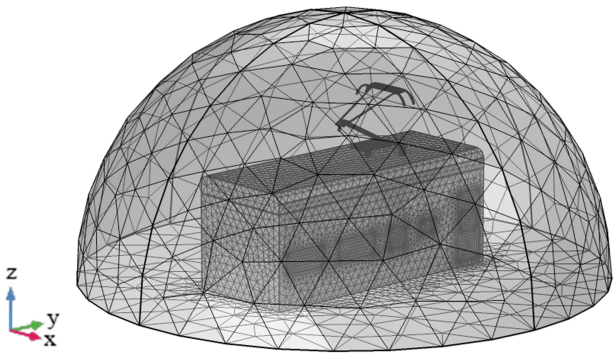

Fig. 4. Model grid division diagram

4. Results and analysis

In this work, the power frequency electric field generated in the EMU carriage under the working state of the pantograph was simulated, then the induced electric field intensity and induced current density in various tissues of four passengers at different positions in the carriage were calculated. Finally, we compared the results with the basic limits of public electromagnetic

exposure in ICNIRP guidelines, so that it can be judged and evaluated whether the power frequency electric field generated by the pantograph will endanger the health of passengers in the EMU carriage.

4.1. Distribution of electric field intensity in the carriage without passengers

Figure 5 shows the distribution of electric field intensity of the pantograph and carriage without passengers in the EMU. As shown in Fig. 5(b), the maximum electric field intensity of the pantograph and the carriage appears at the pantograph insulator and reaches a maximum of 3.799×10^8 mV/m. This paper focuses on the electric field intensity distribution in the carriage. Figure 5(c) points out that the maximum electric field intensity inside the entire carriage is located at the door glass of the carriage shown in Fig. 5, and its maximum value is 1.173×10^6 mV/m. Moreover, the electric field intensity near the window is obviously greater than that inside the carriage.

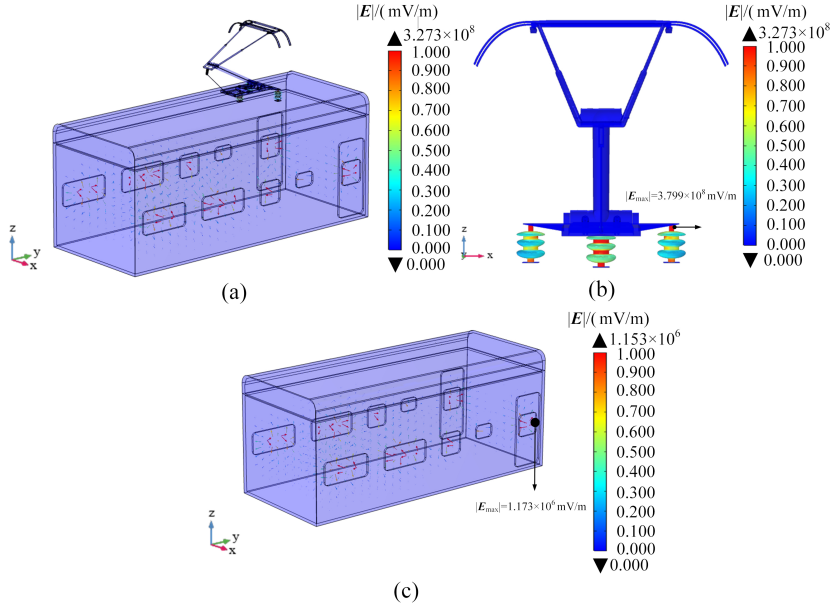

Fig. 5. Electric field intensity distribution of pantograph and carriage without passengers: pantograph and carriage (a); pantograph (b); carriage (c)

Figure 6 shows the electric field intensity distribution in different planes without passengers. As the passenger is seated in the EMU with his head closest to the window, in order to better analyze the electric field distribution here, a cross-sectional plane at $z = 1\,298$ mm in the carriage is intercepted. At the same time, the longitudinal section plane is also taken at $x = 0$ mm on the outer wall of the carriage and $x = 1\,600$ mm in the center of the carriage, as shown in Fig. 3(b). As shown in Fig. 6(a), the electric field intensity near the window is significantly greater than that inside the carriage, with a maximum value of 1.153×10^6 mV/m. It can be seen from Fig. 6(b)

that the aluminum alloy carriage body has good electric field shielding effectiveness, while the shielding effectiveness of windows is poor, the electric field is coupled into the interior of the carriage through the windows and gaps. It can be seen from Fig. 6(c) that although the pantograph is located at the top of the car, the roof deflector and aluminum alloy carriage have good electric field shielding efficiency, the electric field intensity at the center of the carriage is small, with a maximum value of only 3.297×10^3 mV/m.

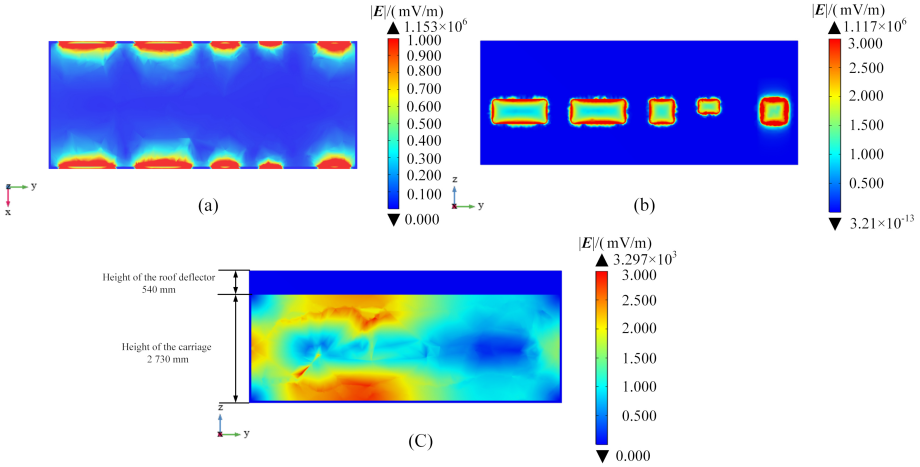

Fig. 6. Electric field intensity distribution in different planes without passengers: at z = 1 298 mm plane (a); at x = 0 mm plane (b); at x = 1 600 mm plane (c)

4.2. Distribution of electric field intensity of human body and carriage with passengers

Since the maximum electric field intensity occurs near the doors and windows, it is likely to cause health hazards to the passengers. Therefore, in order to better study the electric field exposure of passengers in different positions, two human models are placed at the doors, as shown in Fig. 3, to focus on the analysis. At the same time, one human model is placed directly below the pantograph at position B and one at position A.

Figure 7 shows the distribution of electric field intensity inside the carriage in different view directions. The colored arrows in the figure are used to characterize the distribution state of the power lines inside the carriage. From Fig. 7, it can be clearly observed that the electric field generated by the pantograph will be coupled into the internal space of the carriage through the windows, doors and other articulations of the carriage, and the electric field intensity near the windows is obviously larger than that in other areas of the carriage. This is because the EMU carriage is made of aluminum alloy, which has a good shielding effect on the electric field. The material of the window is glass, and its shielding effect of the electric field is poor. At the same time, it should be noticed that the maximum electric field intensity of the entire carriage is located at the door glass of the carriage shown in Fig. 7(b), and its maximum value is 3.195×10^6 mV/m, which is 2.72 times the maximum electric field intensity of the carriage when there is no passenger.

This is because the human body is a medium, which can interfere with the distribution of the original electric field. This phenomenon is noteworthy.

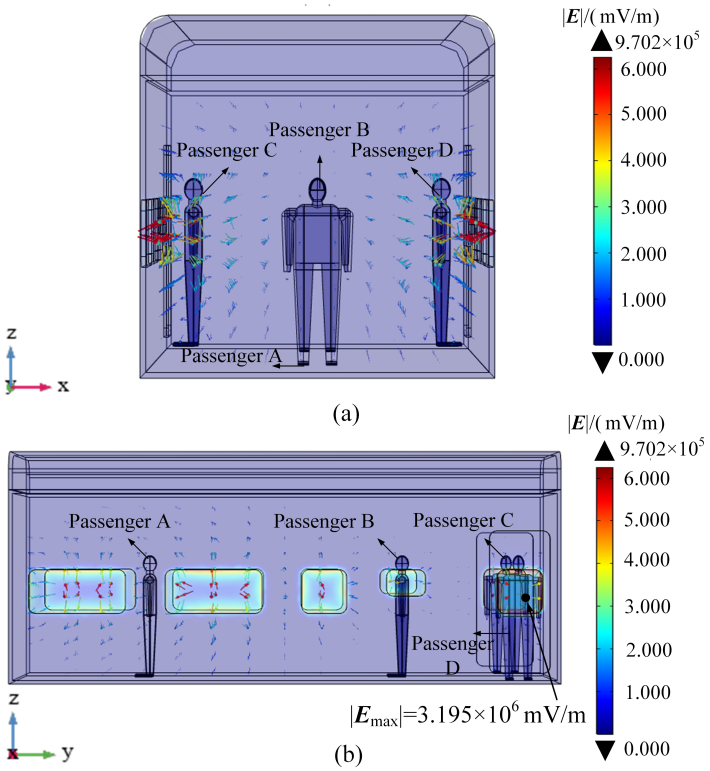

Fig. 7. Electric field intensity distribution in the carriage: front view (a); side view (b)

4.3. *E* and *J* in the passenger's body

4.3.1. *E* in the passenger's body

Figure 8 shows the intensity and distribution of the electric field inside the body of four passengers at different positions in the EMU carriage. The red arrow indicates the direction of the induced electric field intensity in the passenger body. Comprehensive analysis shows that the direction of the induced electric field intensity is from head to foot in the passenger body from top to bottom. At the same time, the maximum induced electric field intensity in the passengers at all four different positions occurs at the sole because the conductivity of the sole is 1×10^{-6} S/m. Among them, the induced electric field in D passenger's sole is the strongest, with a maximum value of 3.028×10^5 mV/m. The maximum induced electric field intensity of A, B and C passengers is 1.592×10^5 mV/m, 1.924×10^4 mV/m, 2.930×10^5 mV/m, respectively.

Figure 9 shows the intensity and distribution of induced current density in the body of four passengers at different positions in the EMU carriage. It can be seen from the diagram that the induced current density inside the body of four passengers at different positions in the EMU

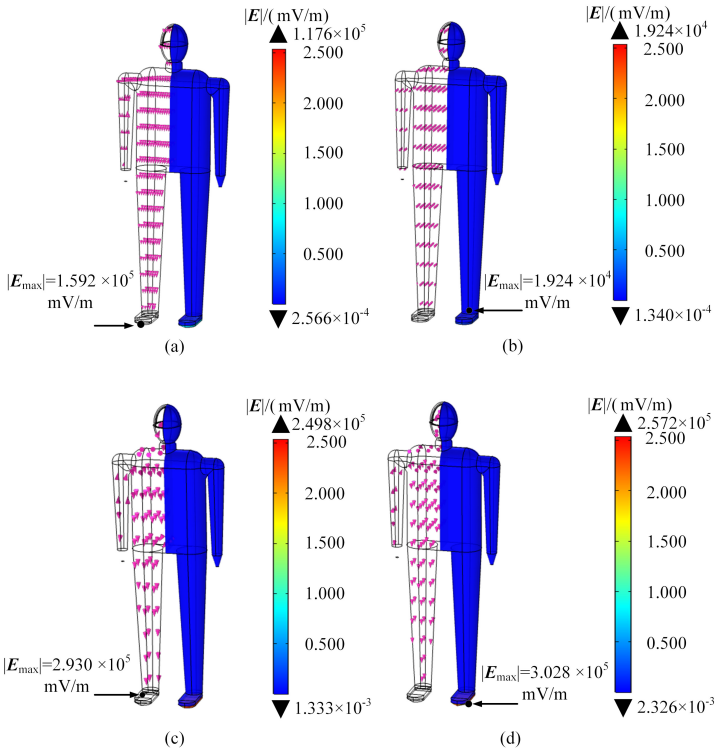

Fig. 8. Distribution of induced electric field intensity in passengers A–D: passenger A (a); passenger B (b); passenger C (c); passenger D (d)

carriage is relatively small, and the maximum value appears at the ankle of C passenger, which is 3.476×10^{-5} A/m^2. The maximum induced current density of A, B and D passengers is 8.293×10^{-6} A/m^2, 2.628×10^{-6} A/m^2, 3.332×10^{-5} A/m^2, respectively.

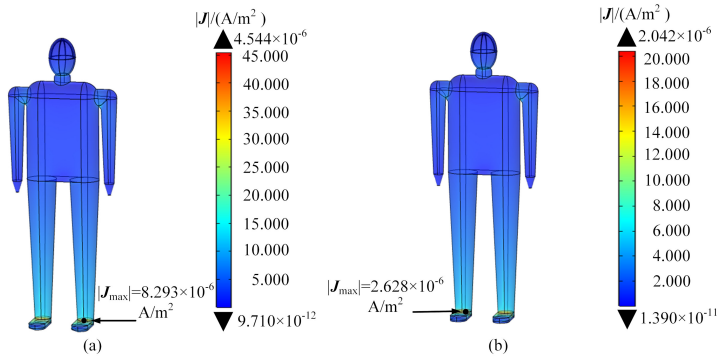

Fig. 9(a), (b)

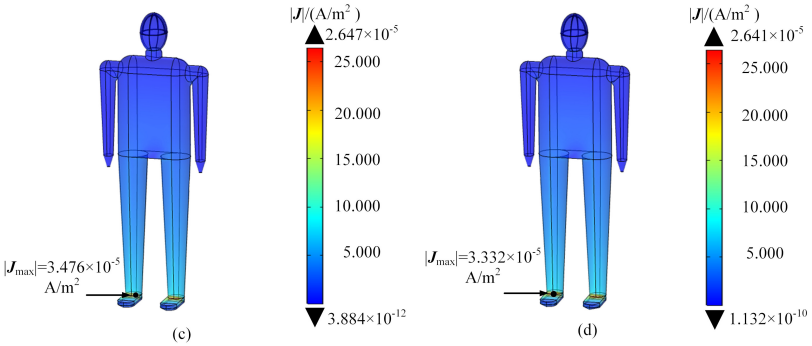

Fig. 9. Distribution of induced current density in passengers A–D: passenger A (a); passenger B (b); passenger C (c); passenger D (d)

4.3.2. *E* in the head of the passengers

Figure 10 shows the intensity and distribution of the electric field intensity induced in the heads of four passengers at different positions inside the carriage. Because of the different positions of the four passengers in the carriage, the screenshots are taken from the left side of each passenger's body to ensure consistency of the discussion. As shown in the figure, the maximum values of the induced electric field intensity in the heads of passengers A, B, C, and D were 54.481 mV/m,

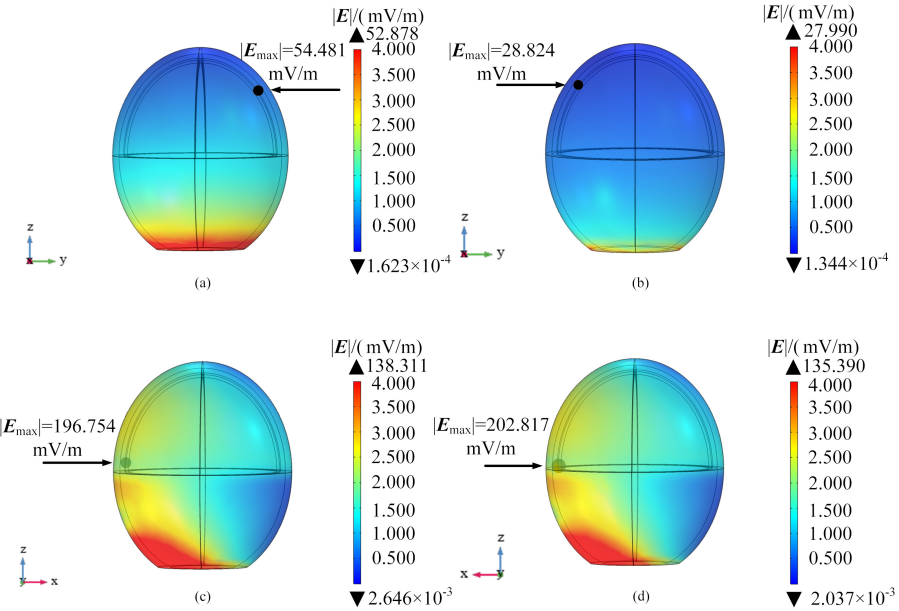

Fig. 10. Distribution of induced electric field intensity in the head of passengers A–D in the carriage: passenger A (a); passenger B (b); passenger C (c); passenger D (d)

28.824 mV/m, 196.754 mV/m, and 202.817 mV/m, respectively. The maximum values of the induced electric field intensity in the heads of all four passengers occurred at the cerebrospinal fluid. This due to the greater electrical conductivity of the cerebrospinal fluid compared to other tissues, producing a higher capacitive reactance similar to that of a capacitor [26, 27]. At the same time, the results are also related to the geometric model of the passenger body and the mesh size factors. The induced electric field intensity in the heads of passengers C, D at the side near the window is obviously larger than that at the side far away from the window, because the pantograph generated by the industrial frequency electric field through the window into the car will be attenuated by the distance.

The brain is one of the most important components of human tissue, so it is necessary to conduct more detailed analysis of the brain in the research. In this paper, the longitudinal section of the passenger's head at different positions is taken to analyze the distribution of the induced electric field intensity of different tissues in the five-layer ellipsoidal model. In order to ensure the consistency of the discussion, the screenshots are placed on the left side of each passenger's head. As shown in Fig. 11, it can be seen from the longitudinal section that the induced electric field intensity in the cerebrospinal fluid area of the passenger's head is the largest among the head tissues. The induced electric field intensity of each organization on the head of passengers at different positions of the EMU carriage is calculated and analyzed in turn, and the specific calculation results are shown in Table 4.

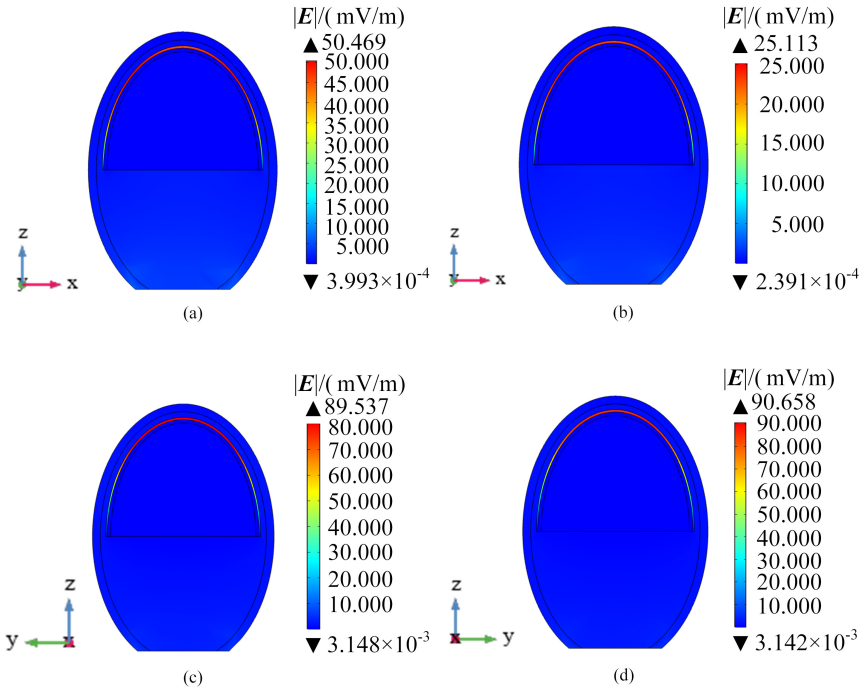

Fig. 11. Distribution of induced electric field intensity in longitudinal section of passenger's head: passenger A (a); passenger B (b); passenger C (c); passenger D (d)

Table 4. $|\boldsymbol{E}_{\max}|$ in different tissues of passenger's head

parameter	Passenger number	Scalp	Skull	Cerebrospinal fluid	Gray matter	White matter
$\|\boldsymbol{E}_{\max}\|$ [mV/m]	A	10.415	15.558	54.481	0.005	0.003
	B	5.068	8.183	28.824	0.003	0.002
	C	24.433	166.988	196.754	0.063	0.034
	D	24.280	202.817	183.957	0.006	0.065

4.3.3. $\boldsymbol{J}$ in the head of the passengers

Figure 12 shows the intensity and distribution of the induced current density in the head of four passengers at different positions inside the EMU carriage. Since the four passengers have different positions in the carriage, in order to ensure the consistency of the discussion, the screenshot from the left side of each passenger's body is selected. It can be seen from the figure that the maximum induced current densities in the head of passengers A, B, C and D are 1.485×10^{-6} A/m^2, 7.228×10^{-7} A/m^2, 4.119×10^{-6} A/m^2 and 5.003×10^{-6} A/m^2, respectively. The maximum value of C and D passengers near the door is obviously larger than that of A and B.

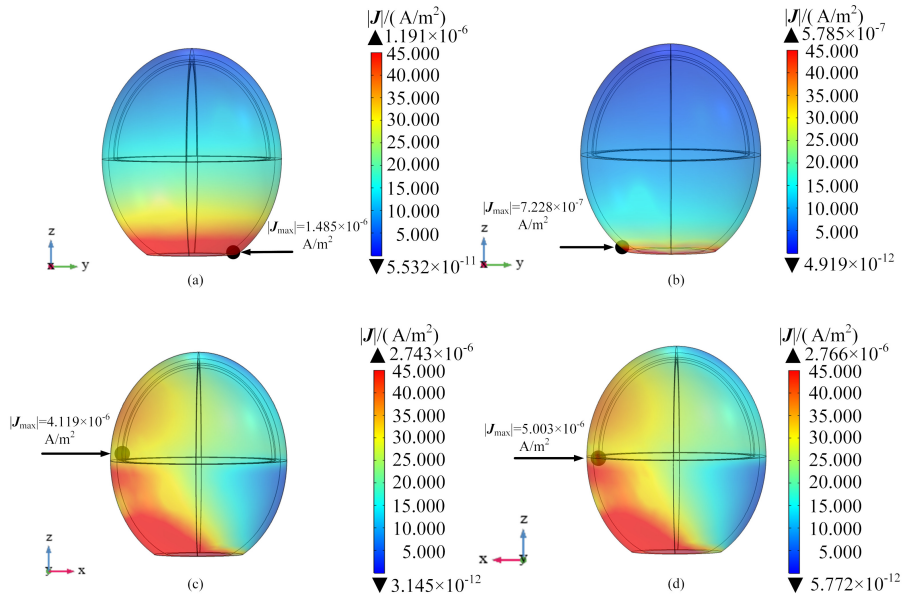

Fig. 12. Distribution of induced current density in the head of passengers A–D in the carriage: passenger A (a); passenger B (b); passenger C (c); passenger D (d)

As shown in Fig. 13, it can be seen from the longitudinal section of the induced current density that the maximum value of the induced current density on this section is located in the

scalp area near the neck of each passenger. The appearance of this result is related to the structure of the model and the mesh size. The narrow surface of the neck is prone to generate electric line aggregation.

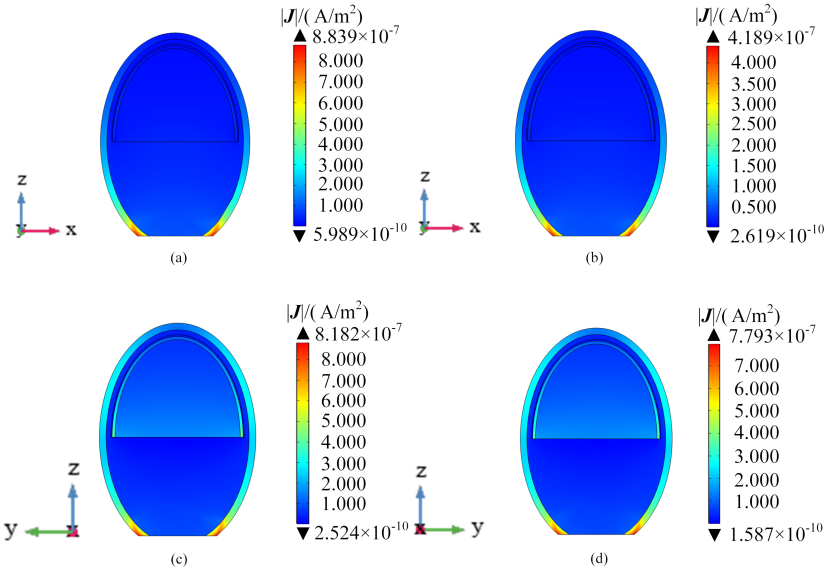

Fig. 13. Distribution of induced current density in longitudinal section of passenger's head: passenger A (a); passenger B (b); passenger C (c); passenger D (d)

5. Conclusions

In this work, the simulation analysis software COMSOL Multiphysics is used to study the induced electric field intensity and induced current density of passengers at different positions in the carriage where the pantograph is located. The analysis and solution results can draw the following conclusions:

1. This work simulated and calculated the electric field intensity of the carriage when there is no passenger in the EMU. The maximum value appears at the door glass as shown in Fig. 5, and its value is 1.173×10^6 mV/m. Then we added the passenger model to the carriage. The maximum electric field intensity of the carriage still appears at the door glass as shown in Fig. 7(b), which is 3.195×10^6 mV/m, 2.724 times the maximum electric field intensity of the carriage without passengers. This is because the human body is a dielectric, which will interfere with the original electric field distribution. This phenomenon deserves attention.
2. We calculated the induced electric field intensity and induced current density of passengers at different positions in the carriage. The maximum induced electric field intensity of passengers at different positions appears at the sole, and the maximum value is 3.028×10^5 mV/m; The maximum induced current density occurs at the ankle, and its maximum value is 3.476×10^{-5} A/m^2.

3. The influence of the electric field environment on human head tissue is emphatically considered. The basic limit of public exposure to the human head and body tissues under a 50 Hz electric field in ICNIRP guidelines is 400 mV/m [14]. When there are passengers in the carriage, the maximum head induced electric field intensity of passengers A, B, C and D are 54.481 mV/m, 28.824 mV/m, 196.754 mV/m, and 202.817 mV/m, respectively, which is far less than the basic limit of ICNIRP public exposure. The maximum induced electric field intensity of the passenger's head at different positions appears in the cerebrospinal fluid region. It is worth noting that the maximum induced electric field intensity of the head of passengers C and D at the door is significantly larger than that of passengers A and B. In order to protect the health of passengers, it is recommended that passengers at the door should not stand for a long time. This recommendation is currently only applicable to CRH5 EMU. This is because the number, size, material and shape of windows will be different due to different vehicle designs, which will affect the distribution of the power frequency electric field in the carriage [28]. The distribution of the power frequency electric field in other vehicles still needs to be further verified.
4. The closer the window is, the greater the induced electric field intensity and the induced current density in the passenger body are. Although the maximum value does not exceed the safety threshold of the ICNIRP guidelines, better shielding measures can be considered at the window to weaken the invasion of the power frequency electric field.

To sum up, the power frequency electric field generated by the pantograph in a working state will not cause harm to the health of passengers in the carriage when passengers take a high-speed EMU. The results of this study are expected to reduce and eliminate the concern and fear of electric field radiation of passengers taking a high-speed EMU in China, and provide a reference for the formulation of electric field exposure standards in China. This work only evaluated the existing carriage of the CRH5 EMU, and the influence of window related parameters on the power frequency electric field will be further studied by our research group in the future work. At the same time, this work only considered the influence of pantographs on power frequency electric field distribution, the influence of traction, contact wire, etc. on the power frequency electric field. The influence of the power frequency magnetic field generated under the working state of pantographs on the health of passengers will also be followed up in future research.

Acknowledgements

This research was financially supported by the National Natural Science Foundation of China (grant nos. 51567015, 51867014) and Gansu Provincial Department of Education: University Teachers' Innovation Fund Project 2023A-034.

References

[1] National Development and Reform Commission of the People's Republic of China, *The Medium and long term railway network Plan* (2016).

[2] Zhang S.G., *CRH5 EMU*, China Railway Press (2008).

[3] Lu M., Ueno S., Thorlin T., Persson M., *Calculating the current density and electric field in human head by multichannel transcranial magnetic stimulation*, IEEE Transactions on Magnetics, vol. 45, no. 3, pp. 1662–1665 (2009), DOI: 10.1109/TMAG.2009.2012770.

[4] Jiang X., An H.J., Peng L., *Research on the amount of cerebral aapoplexy by microwave forward scattering method*, vol. 35, no. 4, pp. 92–96 (2019), DOI: 10.14183/j.cnki.1005-6122.201904019.

[5] Huo X.L., Zhang G.H., Wu C.Z., Zhang C., *Electric field stimulation protects injured spinal cord from secondary inflammatory response in rats*, 39th Annual International Conference of the IEEE Engineering in Medicine and Biology Society, Jeju Island, South Korea, pp. 1958–1961 (2017).

[6] Ohtsuki T., Nabeta T., Nakanishi H., Kawahata H., Ogihara T., *Electric field exposure improves subjective symptoms related to sleeplessness in college students: A pilot study of electric field therapy for sleep disorder*, Immunology Endocrine and Metabolic Agents in Medicinal Chemistry, vol. 17, no. 1, pp. 37–48 (2017), DOI: 10.2174/1871522217666170815163329.

[7] Cieslar G., Sowa P., Sieron K., Sieron A., *Impact of chronic exposure to static, high voltage electric field generated nearby HVDC transmission lines on behavior of rats*, Baltic URSI Symposium, Poznan, Poland, pp. 5–6 (2018).

[8] Wang S., Huang X.H., Li Z.S., Xu J.X., Wang F.X., *Research on electromagnetic exposure measurement method for electric vehicle wireless charging system*, IEEE 2nd International Electrical and Energy Conference, Beijing, China, pp. 513–517 (2018).

[9] Bektas H., Bektas M.S., Dasdag S., *Effects of mobile phone exposure on biochemical parameters of cord blood: A preliminary study*, Electromagnetic Biology and Medicine, vol. 37, no. 4, pp. 184–191 (2018), DOI: 10.1080/15368378.2018.1499033.

[10] Wan S.N., Dang Y.H., Zheng Y.Y., Li J., Zhang J.F., *Investigation on the effect of high frequency electromagnetic radiation on the reproductive health of radar officers and soldiers in a certain army*, Journal of Medical Information, vol. 34, no. 7, pp. 141–142 (2021), DOI: 10.3969/j.issn.1006-1959.2021.07.039.

[11] Xie W.H., Wu G.N., Wei W.F., Yang Z.F., Gao G.Q., *Research on characteristics of the pantograph arc under the action of magnetic field*, IEEE International Conference on High Voltage Engineering and Application, Beijing, China, pp. 1–4 (2020).

[12] Li X., Zhu F., Lu H.D., Qiu R.Q., Tang Y.T., *Longitudinal propagation characteristic of pantograph arcing electromagnetic emission with high-speed train passing the articulated neutral section*, IEEE Transactions on Electromagnetic Compatibility, vol. 61, no. 2, pp. 319–326 (2019), DOI: 10.1109/TEMC.2018.2817578.

[13] Yuan X.L., Tian R., Lu M., *Research on radiation of power frequency electric field in high-speed railway station catenary to workers*, Advanced Technology of Electrical Engineering and Energy (in Chinese), vol. 41, no. 5, pp. 820–888 (2022), DOI: 10.12067/ATEEE2107032.

[14] ICNIRP, *Guidelines for limiting exposure to time-varying electric and magnetic fields (1 Hz to 100 kHz)*, Health Physics, vol. 99, no. 6, pp. 818–836 (2010).

[15] Niu C.X., Han Z.S., Shi L., Lv M., *Shielding simulation of high voltage cable for EMU based on Ansoft Maxwell*, Equipment Manufacturing Technology, no. 12, pp. 117–120 (2021).

[16] Chakarothai J., Arima T., Watanabe S., Uno T., *Exposure evaluation of an actual wireless power transfer system for an electric vehicle with near-field measurement*, IEEE Transactions on Microwave Theory and Techniques, vol. 66, no. 3, pp. 1543–1552 (2018), DOI: 10.1109/TMTT.2017.2748949.

[17] Zhao J., Sun J.J., Jia Z.H., Diao M.F., Liu Y., *Analysis on outer hair cells hazards from occupational exposure to low frequency electric and magnetic fields and magnetic fields and its related factors*, Journal of Clinical Otorhinolaryngology Head and Neck Surgery, vol. 27, no. 22, pp. 1247–1251 (2013), DOI: 10.13201/j.issn.1001-1781.2013.22.001.

[18] Standards Press of China, *Chinese adult body size*, GB/T 10000-1988 (1988).

[19] Tian R., Lu M., *Safety assessment of electromagnetic exposure in high-speed train carriage with full passengers*, Annals of Work Exposures and Health, vol. 64, no. 8, pp. 838–851 (2020), DOI: 10.1093/annweh/wxaa048.

[20] Yang C.Q., Lu M., *Safety evaluation for a high signal operator with electric field exposure induced by contact wires*, Archives of Electrical Engineering, vol. 70, no. 2, pp. 431–444 (2021), DOI: 10.24425/aee.2021.136994.

[21] Stanley R., Daniel A.D., *Current distribution in the brain from surface electrodes*, submitted for publication in Anesthesia and Analgesia.

[22] Wu Z.H., Liu G.Q., Wang J., Liu J.J., Tang J.T., *Human head 3-D finite element model for transcranial electric stimulation*, Journal of Tsinghua University (Science and Technology), vol. 54, no. 9, pp. 1220–1224 (2014), DOI: 10.16511/j.cnki.qhdb.2014.09.023.

[23] Sami G., Lau R.W., Camelia G., *The dielectric properties of biological tissues: III. Parametric models for the dielectric spectrum of tissues*, Physics in Medicine and Biology (in UK), to be published.

[24] Huang X.L., Huang L., Zhou G., Shen J., Dong J., *Research on power frequency electromagnetic environment of UHVAC wires and related electrostatic induction effect*, IEEE Transactions on Magnetics, vol. 47, no. 10, pp. 3516–3519 (2011), DOI: 10.1109/tmag.2011.2149503.

[25] Hu Z.S., *Research on single arm single slide pantograph of 380B high speed EMU*, M.D Thesis, College of Mechanical and Electrical Engineering, Qingdao University, Qingdao (2017).

[26] Du Z.L., Cao Q.S., Lv Z.H., Wang Y., *Precise electromagnetic modeling and simulation of tumor treating fields*, Journal of Clinical Neurosurgery, vol. 19, no. 3, pp. 289–295 (2022), DOI: 10.3969/j.issn.1672-7770.2022.03.010.

[27] Lok E., San P., Hua V., Phung M., Wong E.T., *Analysis of physical characteristics of tumor treating fields for human glioblastoma*, Cancer Medicine, vol. 6, no. 6, pp. 1286–1300 (2017), DOI: 10.1002/cam4.1095.

[28] Lu Y., *Study on shielding effectiveness of carriage for high speed electric multiple units*, M.D Thesis, College of Electronic Information Engineering, Beijing Jiaotong University, Beijing (2017).